JACS
JOURNAL OF THE AMERICAN CHEMICAL SOCIETY
pubs.acs.org/JACS
Article

Ultra-Specific G-Quadruplex–Colistin Interaction for Efficient Transcriptome-Wide G4 Mapping

Shijiong Wei,[#] Xiaobo Zhang,[#] Yilong Feng,[#] Shentong Tao, Dehui Qiu, Xinrong Yan, Guangming Li, Lionel Guittat, Wenli Zhang, David Monchaud, Jean-Louis Mergny, Huangxian Ju,* and Jun Zhou*

Cite This: J. Am. Chem. Soc. 2025, 147, 9962–9971

Read Online

ACCESS | Metrics & More | Article Recommendations | Supporting Information

ABSTRACT: G-quadruplexes (G4s) are challenging targets for chemical biology interventions, notably because of their dynamic topological polymorphism. We found that the antibiotic small-molecule colistin (COL) interacts specifically with a single subtype of G4 structures, the so-called parallel G4s. This interaction triggers the aggregation of the G4/COL complexes in a structure-specific manner, which can thus be separated from the bulk solution by centrifugation. This unprecedented mode of affinity-precipitation was exploited here to design the COL-induced RNA G4 precipitation and sequencing (CoRP-seq) protocol, which allows for the assessment of the prevalence of RNA G4s in the transcriptome of human cells in a straightforward manner. CoRP-seq shines by its ultraspecificity, simplicity, and practical convenience, which thus advances G4 mapping further and addresses unmet needs in the field of G4omics.

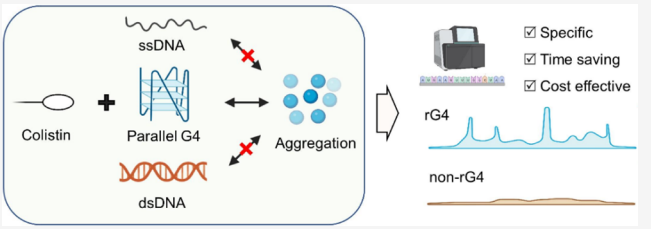

INTRODUCTION

Beyond the canonical double helix of DNA (also known as B-DNA), the alphabet of DNA structures now comprises a dozen letters, including G-DNA (G-quadruplex or G4), H-DNA (triplex), and i-DNA (i-motif).[1,2] These structures fold from repeated sequences, which are both widespread in our genome (covering more than 50%) and located in key regulatory regions.[3,4] Among these non-B-DNA structures, which constitute up to 13% of the human genome,[5] G4s rank high: it is now established that more than one million potential G4-forming sequences can be found in our genome,[6,7] being notably enriched in regions involved in key cellular events (origins of replication, telomere homeostasis, transcription factor recruitment, chromatin organization, etc.).[7−11] G4s fold from guanine (G)-rich sequences; their formation results from the self-assembly of Gs to form G-quartets (via Hoogsteen H-bonds) and the self-stacking of G-quartets (via $\pi-\pi$ stacking) to form the G4 core.[12] The combination of the different structural characteristics of a G4 structure (loop arrangements, glycosidic angles, strand orientation, Figure S1)[13] gives rise to a variety of DNA G4 (dG4) topologies that have been conveniently classified into three categories, i.e., parallel, antiparallel, and hybrid G4s (Figure S1).[14] The study on RNA G-quadruplexes (rG4s) revealed that most adopt parallel G4,[15] with some notable exceptions (i.e., GFP-like fluorescent RNA aptamers such as RNA Mango).[16]

rG4s, like dG4s, play important roles in RNA metabolism for both coding[17−19] and noncoding RNAs.[20,21] Mapping the distribution of rG4s within the human transcriptome has been critical to understanding their functions.[18,22] We and others have developed transcriptome-wide methods to assess the prevalence and functional relevance of rG4s:[23−26] these methods rely on the use of aptamers (L-RNA aptamer),[23] small molecules (TASQs for G4RP),[27−29] or antibodies (BG4 for BG4 uvRIP and rG4IP)[30,31] to capture rG4s and separate the resulting complexes using magnetic beads (MBs) prior to the release of the sequences and their identification by either RT-qPCR or sequencing. These multistep procedures are efficient but technically challenging and time-consuming as well. In addition, the different heating steps required for cross-linking reversal step or release of the RNA samples, for instance, may damage RNA and thus be prone to bias.[32,33] This led us to think about designing an alternative, more straightforward protocol to assess rG4 landscapes transcriptome-wide.

To this end, we report here on the colistin (COL)-mediated purification of rG4s: COL is a cationic decapeptide (Figure 1a) previously used to fight against drug-resistant bacteria.[34,35] Thanks to electrostatic interactions between COL and G4s and efficient $\pi-\pi$ stacking between different COL-bound G4 units, COL can selectively induce the structure-specific aggregation of G4s, especially parallel G4s, from a mixture of nucleic acids (Figure 1a). We thus report on a new method named CoRP-

Received: January 20, 2025
Revised: February 15, 2025
Accepted: February 18, 2025
Published: March 6, 2025

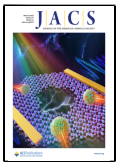

https://doi.org/10.1021/jacs.5c01172
J. Am. Chem. Soc. 2025, 147, 9962−9971

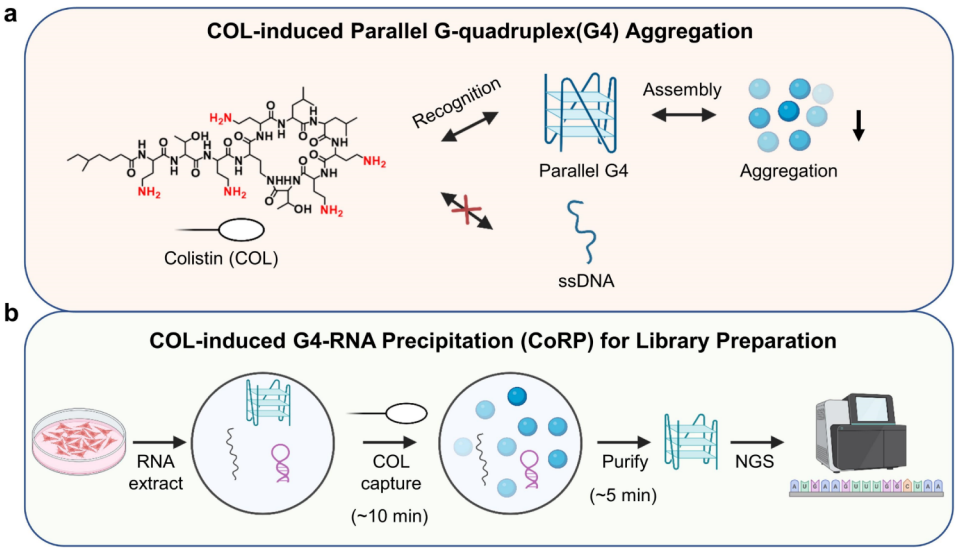

Figure 1. Colistin (COL) selectively induces parallel G-quadruplex (G4) aggregation, which allows for the isolation of rG4s for library preparation. (a) COL induces parallel G4 into aggregation rather than single strand. Amino groups (in red) of COL are the key site to recognize of parallel G4 and regulate the aggregation of G4 and COL. (b) Scheme of COL-induced G4-RNA precipitation (CoRP) for library preparation. COL can isolate rG4 rather than ssRNA or hairpin by structure-specific aggregation from RNA extract of HeLa cells. Enriched rG4 can be easily purified and analyzed on next generation sequencing (NGS).

seq (for COL-induced RNA G4 precipitation and sequencing) that is used here to identify rG4s from HeLa cell lysates without MB purification, within 15 min (Figure 1b). To show its superiority over other techniques, we developed a BG4-based technique referred to as BG4-RIP-seq and systematically compared the results obtained by the two techniques. We found that CoRP-seq, beyond being more practically convenient, also allows for the ultraspecific identification of rG4s from mRNA,[36,37] ncRNA,[23,25] and even the atypical left-handed pUG folds,[38] which were not identified by previous methods. This indicates the great potential of CoRP-seq for transcriptome-wide G4 mapping.

RESULTS AND DISCUSSION

Selectivity of COL for Parallel G-Quadruplex Structures. While thousands of molecules have been tested as G4 ligands, few antibiotics,[39] such as neomycin[40] and distamycin,[41] which are well-known and widely used in traditional pharmacopoeia, were explored. To screen novel G4 ligands from antibiotics, we first assessed here the binding of 8 natural products, including COL, along with vancomycin, thiamphenicol, fluconazole, fosfomycin, kanamycin, tetracycline, and procaine penicillin G (Figure S2), to various DNA structures, including single-stranded DNA (ssDNA), duplex DNA (dsDNA), i-motif, and three different types of G4s (Table S1) by circular dichroism (CD) and UV−vis spectra. After checking antibiotics' spectroscopic suitability (Figures S3 and S4), we found that only COL had a marked effect on G4s (Figures S5−S9): COL indeed drives G4 aggregation, as demonstrated by the turbidification of the solution containing parallel G4 upon addition of COL (Figures 2a and S10), which is not observed with other DNA structures. An analysis by confocal laser scanning microscopy (CLSM) showed that these aggregates have subglobose shapes, with both parallel dG4 and rG4 (Figures S11 and S12).

COL-Driven Parallel G-Quadruplex Aggregation. We next labeled a parallel G4 (here, *N-myc*) or an ssDNA with TAMRA (shown in Table S2), and both of them were mixed with COL. As seen in Figure 2b, bright field imaging confirmed the formation of particles in a structure-dependent manner: only the interaction between COL and TAMRA-modified *N-myc* G4 led to fluorescent particles, demonstrating that COL induced the aggregation of G4 only. This was further substantiated by CD investigations, which showed that the typical G4 CD signal at 263 nm decreased concomitantly with the increase in the typical turbidity signal at 500 nm (Figure 2c). This aggregation was obtained for parallel G4s, including mono- and tetramolecular G4s, inferring that COL induces parallel G4 aggregation regardless of their molecularity (intra- or intermolecular, Figures 2d, S7 and S8). We thus verified that this COL-mediated G4 aggregation is operative with rG4s, given their pervasive parallel topology (Figures 2d, S13 and S14)[18] and also found that it is lost upon sequence mutations that abrogated G4 folding (Figure S15 and Table S3). We also assessed its validity with parallel G4 of inverted helicity (*i.e.*, the left-handed DNA structure ZG4),[42] and the results obtained proved its generality (Figure S16). The interaction between COL and labeled *N-myc* G4 was further characterized by fluorescence titration ($K_{D\ FL}$ = 40.9 nM) and biolayer interferometry (BLI, $K_{D\ BLI}$ = 27.7 nM), while weaker interaction was detectable with nonparallel G4s and random strand (Figures 2e, S17, and S18), which thus confirmed that COL has high affinity and selectivity for parallel G4s.

Detailed Interaction between COL and Parallel G4. To further study the interaction between COL and parallel G4, we first performed fluorescent recovery after photobleaching (FRAP) experiments and found that the fluorescence of the particles formed by *N-myc* G4 and COL can be partly recovered after photobleaching for 100 s, which is similar to phase separation behavior (Figure S19).[43,44] Next, we performed CD and UV titration experiments with different parallel G4s (*N-myc*, Myc2345, c-kit2, CEB25, and RAS; Figure S20): the ellipticity of G4 remarkably decreased with the increase in turbidity; upon addition of COL, the maximum of aggregation being reached at a 5:1 COL:G4 ratio. The stoichiometry of this association was further investigated by

https://doi.org/10.1021/jacs.5c01172
J. Am. Chem. Soc. 2025, 147, 9962−9971

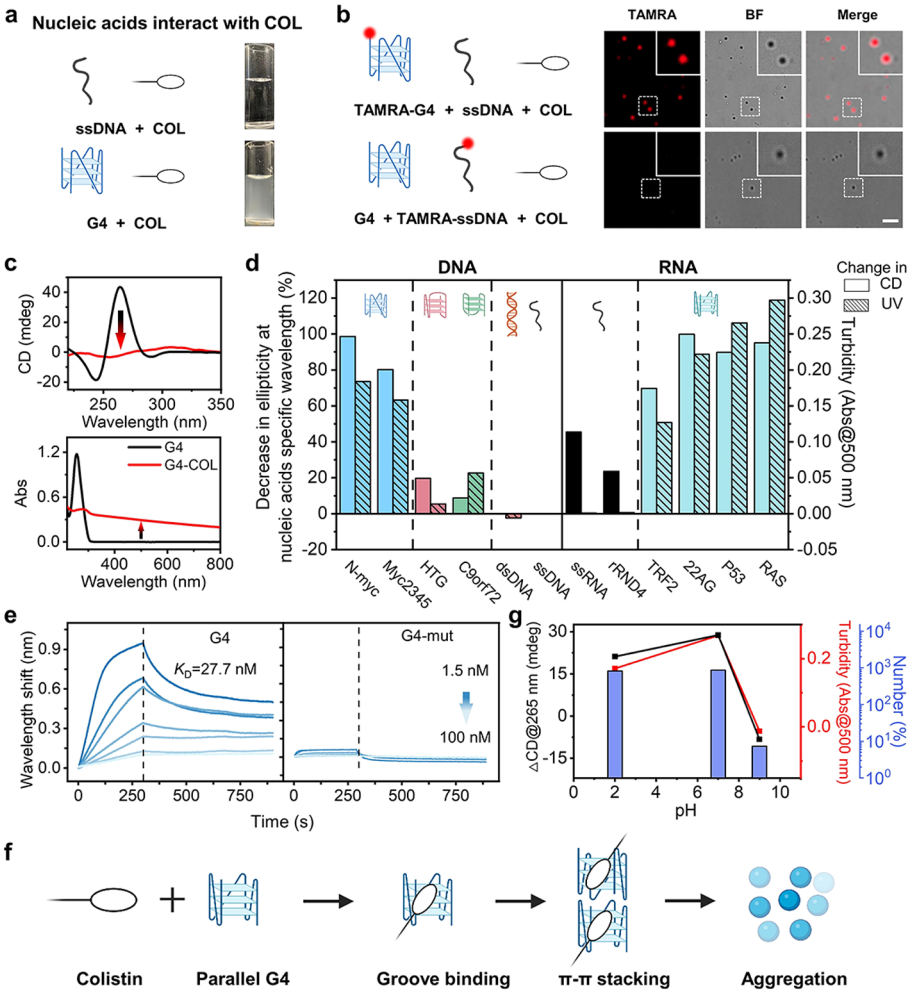

Figure 2. COL selectively induces the aggregation of parallel G4. (a) Photographs of 10 μM ssDNA and parallel G4 DNAs with 50 μM COL. Photographs of other DNA topologies with COL are shown in Figure S10. (b) Mixtures of 5 μM TAMRA-modified *N-myc* G4 and ssDNA or TAMRA-modified ssDNA and *N-myc* G4 with 10 μM COL that lead to the formation of particles. The control data are shown in Figure S11b. Scale bar is 5 μm; "BF" stands for bright field. (c) CD (above) and UV−vis (below) spectra of 5 μM parallel *N-myc* G4 in the absence (black) and presence (red) of 25 μM COL. (d) Topologies dependence of COL. Decrease in ellipticity at nucleic acids specific wavelength (plain bars) and turbidity (500 nm at UV−vis spectra) (striped bars) of different kinds of nucleic acids structures in the presence of COL. The characteristic wavelengths of single-strand, double-strand, i-motif, parallel, hybrid, and antiparallel G4s in CD spectra are 270, 275, 263, 290, and 290 nm, respectively. All sequences are listed in Table S1. (e) BLI binding kinetics of COL to *N-myc* G4 and the *N-myc* mutation sequence. The concentration of COL ranges from 1.5 to 100 nM. (f) Possible progress of COL-induced G4 aggregation. (g) pH dependence of the COL interaction with *N-myc* G4. Different values in CD at 263 nm (black), turbidity (red), and dynamic light scattering (DLS) characterization (blue) of *N-myc* G4 in the presence of COL at pH 2, 7, and 9.

Job plots performed with both *N-myc* and c-kit2 G4s (Figure S21): the 3:1 ratio observed indicates that COL interacts with G4s is multiple, depending on the experimental setup, certainly driven by a dual G-quartet/groove interaction.

COL might thus act as a molecular glue that, through electrostatic interactions, binds simultaneously to the groove of two G4s generating clusters, and $\pi-\pi$ stacking of G4-G4 promotes the aggregation (Figure 2f).[43] To investigate this, we first modified the COL to colistimethate sodium (CMS) and linear peptide (the linear peptide obtained after ring opening of COL): we found that the amino group of COL is the driving force of G4 aggregation and the ring of COL promotes the aggregation (Figure S22). Interestingly, the interaction of COL with parallel G4 was found to be sequence-dependent (Figures S17 and S18), indicating that it recognizes and interacts with the parallel G4 structure only. Taking *N-myc* G4 as a model of parallel G4, we next performed ligand competition with either neomycin,[40] one of the few known G4 groove binders, and ZnDIGP,[45] known to strongly stack atop the accessible G-quartet of a G4: CD, UV−vis, and CLSM results showed a weakened G4 aggregation in the presence of both neomycin and ZnDIGP (Figure S23), suggesting that COL might interact with both groove and G-quartet for triggering G4 aggregation.

To further investigate this, we performed ^{31}P NMR experiments (Figure S24): the chemical shifts of the G4 structure upon COL addition indicate an interaction in close proximity to the phosphate groups of the G4, such as those found in the grooves. In addition, the extension of loop length does not inhibit the aggregation (Figure S25). ^{1}H NMR experiments revealed chemical shifts for H atoms pointing in the grooves (G5, G15, G16, G17, A18, and A19), which was consistent with a groove binding mode (Figure S26).[40,41] Then, we modified c-kit2,[46] a parallel G4 with noncanonical

https://doi.org/10.1021/jacs.5c01172
J. Am. Chem. Soc. 2025, 147, 9962−9971

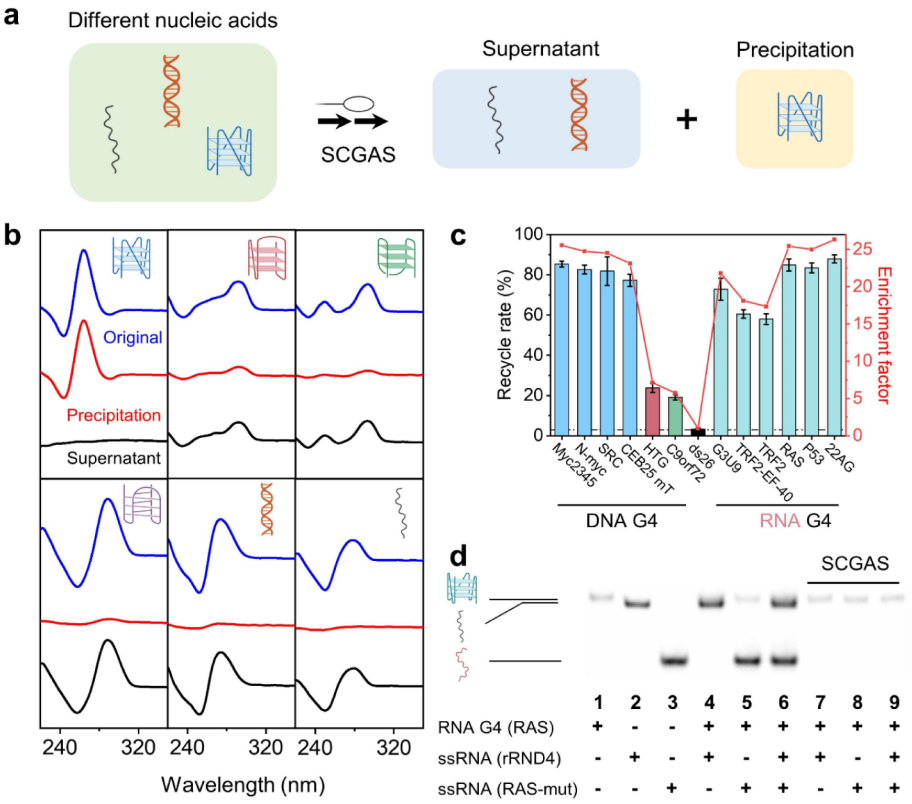

Figure 3. COL can isolate parallel G4s. (a) Schematic representation of the selective COL-induced G4 aggregation separation (SCGAS). (b) Recovery of different DNA structures by the addition of COL. CD spectra demonstrated that parallel G4s can be completely recovered, while other DNAs still remain in the supernatant. (c) Recycle rate (%) and enrichment factor of different nucleic acids by SCGAS. From left to right: DNA G4s contained parallel G4s (in blue), hybrid G4 (in begonia red), antiparallel G4 (in green); hairpin (in black); RNA G4s are in light blue. Note: CEB25 mT is a DNA G4 sequence with a long loop; G3U9 and TRF2-EF-40 are RNA G4 sequences with long loop and flank, respectively. (d) Native polyacrylamide gel electrophoresis displayed selective capture of parallel G4 among different structural nucleic acids mixed sample by SCGAS. Lanes 1−3 were RNA G4 (RAS) and two linear RNA (rRND4 and RAS-mut), respectively; lanes 4−6 were RNA G4 mixed with rRND4, RAS-mut and both of them, respectively; lanes 7−9 displayed mixed sample from lanes 4−6 were treated by SCGAS, and then resuspending from precipitations were visualized. All sequences are listed in Table S1.

base pairs stacked on a terminal G-quartet: G4 aggregation becomes more pronounced when these base pairs are mutated and the terminal G-quartet is fully exposed (Figure S27). Altogether, these results infer that the aggregation of parallel G4s selectively induced by COL likely originates in its ability to associate G4s via groove binding and make the resulting multi-G4 edifices stable thanks to efficient $\pi-\pi$ stacking between their terminal G-quartets (Figure 2f).[43,44]

Controlling COL-Promoted G-Quadruplex Aggregation. Given that the concomitant decrease in ellipticity and increase in turbidity described above remarkably relate to the aggregation events (Figure S28), we used them to assess how the experimental conditions governed COL-mediated G4 aggregation. First, we studied the effect of pH: dynamic light scattering (DLS), CD, and UV−vis analyses showed that the particles were formed under neutral and acidic, but not basic, conditions (Figures 2g and S28−S30), likely because of the protonable residues of COL ($pK_a \sim 10$), which trigger electrostatically and $\pi-\pi$ stacking-driven G4 aggregation (discussed above) only when protonated (below pH ∼ 8).[47] Then, we studied the effect of cations: we found that COL-mediated G4 aggregation is ion-independent, occurring in the presence of K^+, Na^+, and Li^+ (Figures S31−S33), which thus highlighted that the aggregation is primarily driven by the G4/COL association. Finally, the stability of the G4/COL particles was found to decrease with temperature, in the temperature range where the G4 melts (Figure S34), demonstrating that G4 formation is critical for aggregation. It should be noted that COL differs from other ligands affecting the properties of G4, as it neither stabilizes G4 nor promotes G4 formation, as confirmed by thermal, NMM and ThT fluorescence imaging, G4-forming dependence, and enzyme inhibition experiments (Figures S34−S37 and Table S4). Collectively, these experiments demonstrated that G4/COL aggregation can be fully harnessed, being regulated by pH, heat, and ionic conditions.

Parallel G-Quadruplex Topology Sorting. We further exploited this specific, strong, and reversible association and designed an assay termed selective COL-induced G4 aggregation separation (SCGAS, Figures 3a and S38). Upon interaction with COL, G4-based spherical particles rapidly form in neutral solution (<5 min) and quickly dissociate/reassociate (<1 min) upon pH variations from 9 to 7 (G4s are stable at pH 9, Figure S29), in a manner that is both repeatable (Figure S39) and specific for parallel G4s (Figure 3b) without RNA degradation during resolubilization (Figure S40). Indeed, the SCGAS reversibility reaches >60% with parallel dG4s and rG4s (i.e., Myc2345, *N-myc*, SRC, TRF2, RAS, P53, and 22AG) versus <20% for HTG, C9orf72, and ds26 (Figure 3c). We thus performed SCGAS in a competitive manner (i.e., with a mixture of parallel and antiparallel G4s) (Figure S39). This demonstrated the specificity for parallel G4 of the COL-induced G4 aggregation, even with the highly polymorphic

https://doi.org/10.1021/jacs.5c01172
J. Am. Chem. Soc. 2025, 147, 9962−9971

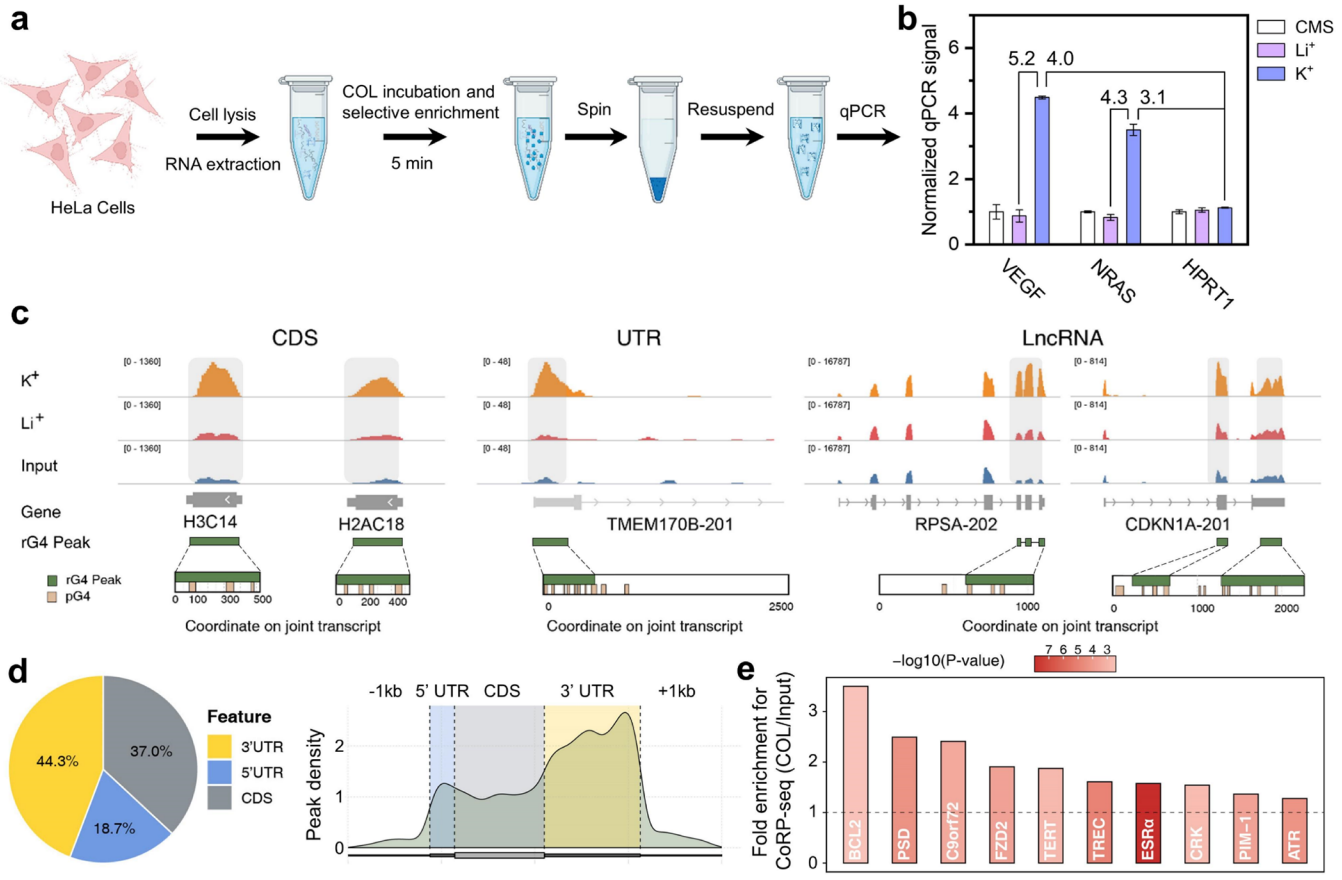

Figure 4. Whole-genome rG4 mapping by COL-induced RNA G4 precipitation and sequencing (CoRP-seq). (a) Schematic representation of the isolation of G4 targets from HeLa cell extracts using COL-induced G4-specific precipitation (CoRP). (b) CoRP signals of control versus COL through RT-qPCR quantification of VEGF, NRAS, and HPRT1 mRNA levels. The qPCR signal is normalized to the CMS group, and the folds of enrichment are labeled in the figure. (c) A representative integrative genomics viewer (IGV) snapshot of CoRP-seq library including K^+ treated (orange), Li^+ control (red), and input (blue). Enrichment of rG4 in CDS (left), UTR (middle), and reported lncRNA (right). Barplot (bottom) shows the joint transcript coordinates. Rectangle bars represent rG4 (top, green) region and predicted G4 (pG4) (bottom, yellow) region. pG4 sequences are obtained by hierarchical assignment using hg38 reference gene as descried in Materials and Methods section. Whether CoRP-seq can enrich G4-forming sequences was estimated by rG4 region matches with pG4 or not. (d) Pie (left) and density plots (right) show peak density of rG4 in different region of mRNA. (e) Fold enrichment of reported genes contained rG4 for CoRP-seq. The vertical axis indicates fold enrichment (COL/input) and the color represents $-\log_{10}$ (p-value).

human telomeric G4[48] (Figures S41, S42, and Table S5). We also showed that SCGAS is able to discriminate a DNA G4 (Myc2345) from ssDNA (A20) and dsDNA (ds17) (Figure S43) and that it works with RNA G4s as well, being specific for rG4s over ssRNA (Figure 3d), even in a competitive context (10-fold excess; Figure S44). To go a step further toward biological applications, we included a rG4-forming sequence embedded in a longer RNA fragment, designing TRF2 with flanking extensions of 10, 20, and 40 nucleotides (i.e., TRF2-EF-10, 20, and 40, respectively) along with its mutated, non-rG4-forming analog TRF2-EF-40-mut (Figure S45 and Table S3): we found that SCGAS works quite well with these longer sequences, again in a highly G4-specific manner (Figure 3c).

CoRP-Seq Identifies Transcriptome-Wide RNA G4s. We next investigated the reliability of COL-induced RNA G4 precipitation (CoRP) in human cells (HeLa cells). The schematic representation of the CoRP protocol can be seen in Figure 4a: briefly, RNA extracts from HeLa cell lysates were incubated with a high concentration of COL (100 μM) for 5 min before the isolation of the COL/rG4 complexes by centrifugation; next, these samples were resuspended in 10 mM Tris-HCl buffer containing 100 mM LiCl, and the pH was adjusted to 8.8 to dissociate the aggregates before the isolation of the RNA fragments using TRIZOL (Figure S46). We first assessed the efficiency of the CoRP protocol by RT-qPCR using two well-known rG4-containing mRNAs, NRAS and VEGF, and an unstructured RNA control, HPRT1. Compared with HPRT1 in the K^+ treated condition, NRAS was 3.1-fold enriched when normalized against CMS (control), while VEGF was 4.0-fold enriched (Figure 4b and Table S6). The G4 nature of these transcripts was confirmed by the modulation of the cationic content of the CoRP buffers, the qPCR signals being higher in K^+ versus Li^+ buffers, for both NRAS (4.3-fold) and VEGF (5.2-fold) (Figure 4b). These results thus showed that the CoRP-RT-qPCR method is suited to the identification of biologically relevant rG4-containing RNA sequences from HeLa cells.

Next, we implemented CoRP-seq to map rG4s transcriptome-wide (Figures S47): two biological replicates were conducted in K^+- and Li^+-rich conditions (along with an input control), and high correlation coefficients were obtained for each treatment (Figure S48). We found 6,959 rG4 peaks (relative to input) common to the biological replicates in K^+-rich conditions: most rG4 peaks corresponded to protein-

https://doi.org/10.1021/jacs.5c01172
J. Am. Chem. Soc. 2025, 147, 9962−9971

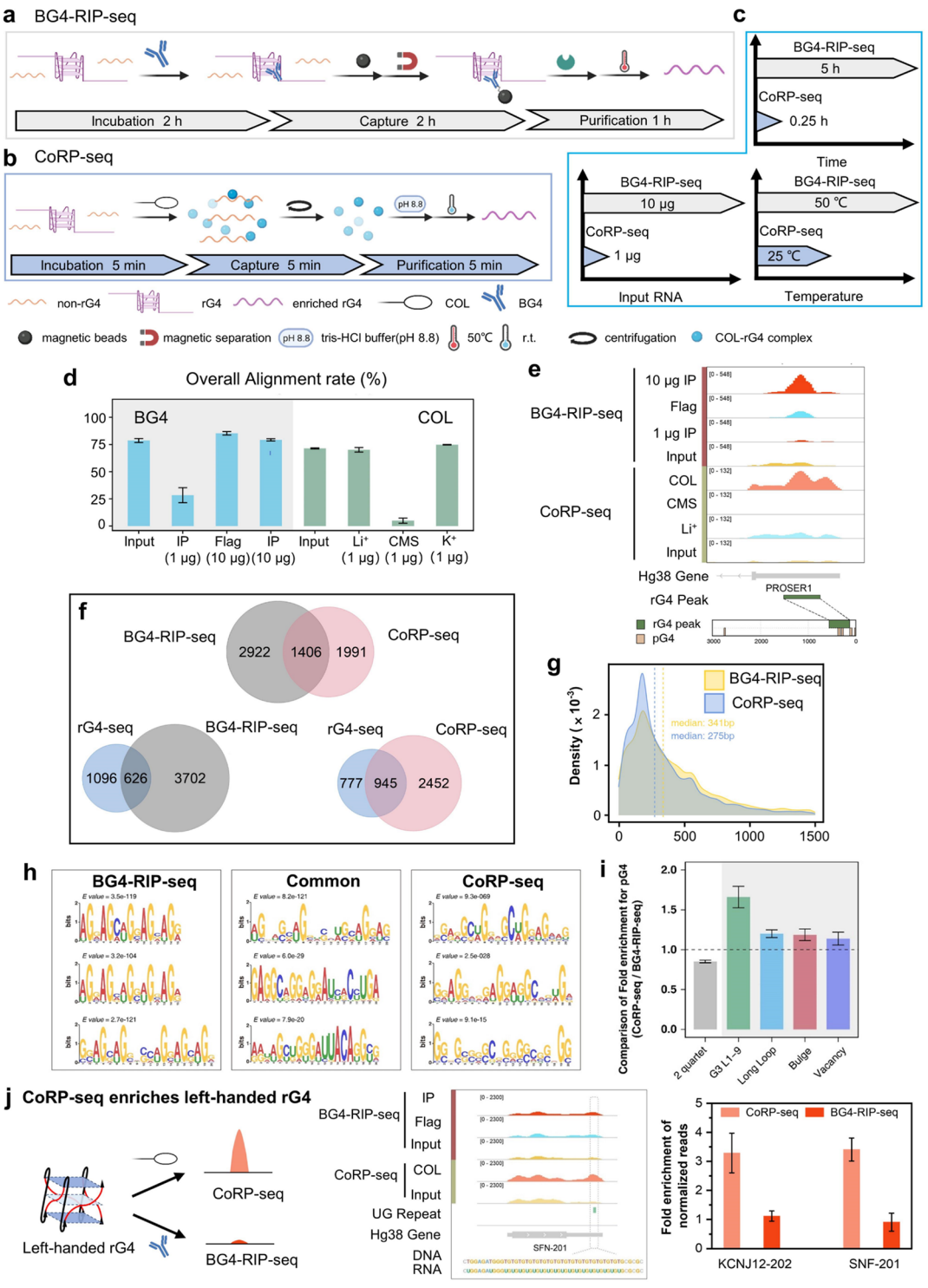

Figure 5. rG4 mapping using CoRP-seq and BG4-RIP-seq. Schematic library preparation workflows of (a) BG4-RIP-seq and (b) CoRP-seq. (c) Comparison of sample preparation time, input RNA, and purification temperature of workflow in BG4-RIP-seq and CoRP-seq. (d) Comparison of overall alignment between BG4-RIP-seq (left) with initial amount of 1 and 10 μg total RNA input relative to controls (input and flag) and CoRP-seq (right) with initial amount of 1 μg total RNA relative to controls (input, Li^+, and CMS). (e) A representative integrative genomics viewer (IGV) snapshot of CoRP-seq and BG4-RIP-seq in PROSER1 region. (f) Pairwise comparisons of enriched sequences for CoRP-seq (1 μg input RNA) relative to input, BG4-RIP-seq (10 μg input RNA) relative to input, and rG4-seq; rG4-seq data were from Gene Expression Omnibus GSE77282. (g) Length distribution of G4 peaks detected using CoRP-seq (blue) and BG4-RIP-seq (yellow). (h) Motif discovery using MEME for CoRP-seq and BG4-RIP-seq peak data sets. (i) The ratio of frequency of CoRP (1 μg input RNA) and BG4-RIP (10 μg input RNA) in different G4 structures, and frequency is calculated the fold enrichment of rG4 compared to randomly selected transcript sequences. The values were present as mean ± sd, n = 10. When the ratio is larger than 1, it means CoRP enriches more in this G4 structure than BG4-RIP; conversely, BG4-RIP prefers that G4 structure. (j) Enrichment of rG4 in 3′ UTR region with $(GU)_n$ motif, which can form left-handed G4 (n > 12). Middle: IGV snapshot of CoRP-seq and BG4-RIP-seq in SFN-201 region; right: fold enrichment of normalized read counts by CoRP-seq (1 μg input RNA) versus input and BG4-RIP-seq (10 μg input RNA) versus Flag in the KCNJ12-202 and SFN-201 region.

https://doi.org/10.1021/jacs.5c01172
J. Am. Chem. Soc. 2025, 147, 9962−9971

coding mRNA (69.9%) and 22.7% to noncoding RNA (Figure S49). The integrative genomics viewer (IGV) analysis seen in Figure 4c showed a notable enrichment of rG4s in K^+- versus Li^+-rich conditions and input, and an excellent match with predicted G4 (pG4) sequences (using fastaRegexFinder). Besides coding sequences (CDSs) and untranslated regions (UTRs), several noncoding RNAs with previously reported rG4[18] have also been identified, suggesting the accuracy of rG4 mapping by CoRP-seq (Figures 4c and S50). Also, CoRP-seq even enriched left-handed rG4s folding from $(UG)_n$[36] sequences, which was confirmed by RT-qPCR and CD spectra (Figures S51−S53 and Table S4). These results indicate that the CoRP protocol is unique in its ability to capture rG4s. The distribution of rG4s across the RNA transcripts was uneven, being mostly located in 3′-UTR (44.3%) versus CDS (37.0%) and 5′-UTR (18.7%, Figure 4d). To further confirm the accuracy of the identification of rG4, three G4-containing (positive) *loci* and two *loci* devoid of G4 (negative) were evaluated by CoRP-RT-qPCR (Table S6), and we found that positive *loci* were strongly enriched (3.8- to 4.5 fold) relative to negative *loci* (Figure S52). Of note, the G4 nature (or not) of the positive and negative *loci* was verified by CD (Figure S54 and Table S7). The gene ontology (GO) analysis of the rG4-containing transcripts was displayed in Figure S55 and Table S8. Furthermore, several reported genes (e.g., BCL-2, PSD) containing G4-forming sequences were enriched by CoRP-seq (Figure 4e).[18,36] Collectively, all the above results confirm that the quality of our rG4 data can be justified for the downstream assay.

Comparison of CoRP-Seq and BG4-RIP-Seq. The efficiency of CoRP-seq was thus compared with an alternative BG4-based technique that we refer to as BG4-RIP-seq (Figure 5a−c). In this protocol, we employed 3 μg of BG4 antibody for 10 μg fragment RNA incubated at 150 mM K^+ (along with input and flag controls), performing two biological replicates. After capture by MB and purification by heat and proteinase K treatments, enriched RNAs were handled as previously described.[31] BG4-RIP-seq led to the identification of rG4 in the 10 μg input RNA with over 20 million RNA-obtained sequence reads and >75% mapped ratio (Figures 5d and S56). An IGV snapshot of BG4-RIP-seq displayed a notable enrichment of rG4s relative to the input control (Figure 5e). We found that only 41.3% of detected genes were common to CoRP-seq and BG4-RIP-seq relative to input (Figures 5f and S57). We also compared enriched genes with rG4-seq and found that BG4-RIP-seq and CoRP-seq have 626 and 945 common G4 sequences compared with rG4-seq, respectively (Figure 5f). This result is interesting, as the overlap is indeed significantly higher with CoRP-seq, possibly highlighting the advantage of this method to identify true G4-forming motifs.

To understand this difference, we investigated the length distribution of G4 peaks and found that the G4 peak distribution is wider for BG4 (average length: 341 bp) than for COL (average length: 275 bp), likely originating from a significant difference in capture efficiency (Figure 5g). Motif analysis showed that BG4-RIP-seq prefers 2-quartet rG4s and those that fold from $(GGA)_n$ repeats, while CoRP-seq prefers 3-quartet rG4s (Figures 5h,i, and S58). Quite uniquely, CoRP-seq enriches left-handed rG4 found in KCNJ12-202 and SFN-201 (3.3- and 3.4-fold relative to input, respectively) regions where BG4-RIP-seq shows less enrichment (Figures 5j and S51). Therefore, the differences between the two molecular tools BG4 and COL likely result from a difference in G4 binding, COL primarily interacting with parallel G4s (without induction and/or stabilization), while BG4 is a pan-G4 interacting agent, enriching G4s whatever the nature of their G4 fold.[49]

All CoRP-seq libraries demonstrated excellent sequencing correlations and a high level of reproducibility, even with an amount of input RNA as low as 1 μg, which is one tenth of the amount required for BG4-RIP (see the principal component analysis in Figure S47). To better highlight this difference, we performed BG4-RIP-seq with only 1 μg of RNA and obtained low quality results, both in terms of mapping (<30%) and sequence reads (<10 M; Figures 5d,e, S47, and S56); in contrast, when performed with 0.5 μg, CoRP-seq led to high mapping (75%) and sequence reads (45.1 million) (Figure S59), confirming its higher sensitivity and practical convenience.

CONCLUSION

We benefit here from the quite unique G4-recognizing properties of COL (that is, its ability to interact with and aggregate parallel G4s only) for further advancing the G4 sequencing arsenal. The origins of these unique properties remain speculative at this stage, but chemical modification experiments along with NMR data point toward a groove binding, which leads G4/COL complexes to readily aggregate between accessible G-quartets via $\pi-\pi$ stacking, or via a COL molecular glue effect,[43] making the resulting supramolecular assemblies easily isolable by centrifugation. We thus showed here that COL effectively precipitates parallel G4s only, both dG4s and rG4s, and that this unprecedented affinity capture method could be used both in vitro via the selective COL-induced G4 aggregation separation (SCGAS) protocol, and with cell lysates via the COL-induced G4 RNA-specific precipitation (CoRP) protocol, implementable in both RT-qPCR and sequencing-based versions (CoRP-seq). The former, SCGAS, is a reliable way to separate different dG4/rG4 topologies from nucleic acid mixtures in vitro and represents a new solution to govern G4 topology of polymorphic and highly dynamic structures; the latter, CoRP-seq, represents a real breakthrough in the field of G4 sequencing as it does not involve the heterogeneous magnetic bead (MB)-based isolation of captured G4-forming sequences, as do the competitive techniques G4RP-seq and BG4-RIP-seq. CoRP-seq offers an alternative way to sequence RNA G4s, which is not only easier and faster but also less expensive and experimentally independent than previously reported methods.

From a more technical point of view, the total time of the CoRP protocol is 0.25 h from incubation, G4 fragment capture, to purification, which has to be compared with the 5 h required between the same steps for the BG4-RIP protocol (Figure 5c). Also, the purification of the enriched RNA samples is performed at room temperature for CoRP versus 50 °C for BG4-RIP. Given the known fragility of RNAs (Figure S60), shorter and softer protocols are thus to be favored, as they might portray the rG4 landscapes more accurately. The CoRP-seq protocol is simple to implement and allows for avoiding RNA degradation; it is also highly sensitive as the direct comparison with BG4-RIP-seq indicates that the minimal RNA amount requested for reliable experiments for CoRP-seq is roughly one tenth of that required by BG4-RIP-seq. Moreover, CoRP-seq identified most of the rG4 peaks located in UTR distribution, which is in agreement with rG4-seq (the reference technique based on reverse transcriptase

https://doi.org/10.1021/jacs.5c01172
J. Am. Chem. Soc. 2025, 147, 9962−9971

(RT)-stalling profiling),[23] but the proportion of rG4s in CDS has increased compared with rG4-seq. CoRP-seq thus represents an important step forward in the simplification of in vitro rG4 mapping techniques. This makes CoRP techniques (CoRP-RT-qPCR and CoRP-seq) accessible to all, which is the surest pledge for democratizing, that is, advancing and boosting G4 research further.

MATERIALS AND METHODS

Specificity Experiments. The sequences of the DNA and RNA oligonucleotides used herein are given in Table S1. The preparation of these sequences is described in the Supporting Information, Methods section. The CD spectra were collected from 220 to 350 nm, and UV−vis spectra were recorded from 220 to 800 nm. To simply analyze and compare UV−vis and CD data, we chose the change in the strongest bands in CD spectra (e.g., 263 or 290 nm depending on G4 structures) and the absorbance at 500 nm (turbidity) of respective nucleic acid structures to judge the degree of binding between DNA and antibiotics. The specific wavelengths of single-strand DNA (ssDNA) and RNA (ssRNA), double-strand DNA (dsDNA), i-motif, parallel G4, hybrid G4, and antiparallel G4 in CD spectra are 270, 270, 275, 263, 290, and 290 nm, respectively. The decrease in ellipticity at DNA and RNA specific wavelengths (%) obtained by CD spectra at characteristic wavelengths was calculated as eq 1:

$$\frac{CD_{DNA/RNA} - CD_{DNA/RNA-5COL}}{CD_{DNA/RNA}} \times 100\% \quad (1)$$

where $CD_{DNA/RNA}$ and $CD_{DNA/RNA-5COL}$ indicate CD spectra of 5 μM DNA or RNA at the specific wavelengths in the absence and presence of 25 μM COL.

Selective Colistin-Induced G-Quadruplex Aggregation Separation (SCGAS). The sequences of the oligonucleotides used here are given in Table S3. The in vitro G4 capture experiments were performed in a 500-μL final volume as follows: first, the 25 μM COL was added with oligonucleotides (5 μM), and the mixture solution was stirred for 30 s and incubated at 25 °C for 5 min. To this end, the mixture solution was centrifuged for 5 min (10000 r.p.m.), and the supernatant was removed while the precipitate was resuspended in 500 μL of 10 mM Tris-HCl buffer (pH 8.8, 100 mM LiCl). The absorbance of the resuspended solution was collected by a Cary 3500 UV−vis spectrophotometer. The control oligonucleotides were prepared as above except for the addition of COL and were kept in 500 μL of 10 mM Tris-HCl buffer (pH 8.8, 100 mM LiCl). This allowed for a direct quantification of the COL capture efficiency. To account for the difference in nucleotides, the concentrations of nucleic acid in long loop and long groups and colistin were calculated by the phosphate group, $[c^-]$, and amino group, $[c^+]$, respectively. The concentrations of both $[c^-]$ and $[c^+]$ are 100 and 125 μM, respectively. All experiments were performed in triplicates.

Competitive experiments were performed with COL (25 μM), G4 (5 μM), and the nucleic acid competitors (5 μM). The capture process was performed as above. All supernatants were diluted five times, and control samples were 1 μM. The pull-down assay in the mixture was visualized in 10% native polyacrylamide gel (PAGE) at 130 V for 45 min. The PAGE image was acquired with a ChemiDoc MP Imaging System (Bio-Rad, USA) before staining with SYBR Gold Nucleic Acid Gel Stain for 20 min.

COL-Induced G4 RNA-Specific Precipitation (CoRP). HeLa cells were scraped and resuspended in TRIZOL and then sonicated using a Covaris M220 Ultrasonicator with default settings at 10% duty for 5 min. Fragmented RNA (100−500 nt) was extracted using the manufacturer's instructions. The 2 μg total RNA sample was then divided into two parts for 150 mM Li^+ and 150 mM K^+ in cacodylic acid buffer at 60 °C for 5 min, then slowly cooled down to room temperature. Five percent of the incubated sample was collected as the input control. Next, samples were incubated with 100 μM COL for 5 min after being diluted in 10 mM of Li^+ or K^+. COL-containing samples were centrifuged for 5 min (4 °C, 10000 rpm), and the supernatant was removed. The precipitate was resuspended with 10 mM Tris-HCl buffer (pH 8.8, 100 mM LiCl) and then extracted using the Qiagen RNeasy Plus Mini Kit following the manufacturer's protocol. All experiments were performed in triplicate.

Figures' Design. All of the plots were generated by Prism, R, ImageJ, and Origin software, and the schematic representations were created by BioRender.com.

ASSOCIATED CONTENT

Data Availability Statement

The sequencing data have been deposited into NCBI's Gene Expression Omnibus and are accessible at GSE260479.

Supporting Information

The Supporting Information is available free of charge at https://pubs.acs.org/doi/10.1021/jacs.5c01172.

Additional experimental details, materials, and methods, including oligonucleotide sequences used in the study; the interactions between G4 and COL analyzed by UV−vis, CD, NMR, BLI, fluorescence and gel electrophoresis; the properties of aggregation measured by DLS, CLSM imaging and FRAP; rG4 enrichment validated by RT-qPCR; establishment of CoRP-seq and BG4-RIP-seq, and statistical analysis. The file also contains Supplementary Figures S1−S60 and Tables S1−S8 (PDF)

AUTHOR INFORMATION

Corresponding Authors

Huangxian Ju − *State Key Laboratory of Analytical Chemistry for Life Science, School of Chemistry and Chemical Engineering, Nanjing University, Nanjing 210023, China;* orcid.org/0000-0002-6741-5302; Email: hxju@nju.edu.cn

Jun Zhou − *State Key Laboratory of Analytical Chemistry for Life Science, School of Chemistry and Chemical Engineering, Nanjing University, Nanjing 210023, China;* orcid.org/0000-0002-6793-3169; Email: jun.zhou@nju.edu.cn

Authors

Shijiong Wei − *State Key Laboratory of Analytical Chemistry for Life Science, School of Chemistry and Chemical Engineering, Nanjing University, Nanjing 210023, China*

Xiaobo Zhang − *State Key Laboratory of Analytical Chemistry for Life Science, School of Chemistry and Chemical Engineering, Nanjing University, Nanjing 210023, China;* orcid.org/0000-0003-0222-2515

Yilong Feng − *State Key Laboratory for Crop Genetics and Germplasm Enhancement and Utilization, CIC-MCP, Nanjing Agricultural University, Nanjing 210095, China*

https://doi.org/10.1021/jacs.5c01172
J. Am. Chem. Soc. 2025, 147, 9962−9971

Shentong Tao − *State Key Laboratory for Crop Genetics and Germplasm Enhancement and Utilization, CIC-MCP, Nanjing Agricultural University, Nanjing 210095, China*
Dehui Qiu − *State Key Laboratory of Analytical Chemistry for Life Science, School of Chemistry and Chemical Engineering, Nanjing University, Nanjing 210023, China*
Xinrong Yan − *State Key Laboratory of Analytical Chemistry for Life Science, School of Chemistry and Chemical Engineering, Nanjing University, Nanjing 210023, China;* orcid.org/0009-0003-5574-2546
Guangming Li − *State Key Laboratory of Analytical Chemistry for Life Science, School of Chemistry and Chemical Engineering, Nanjing University, Nanjing 210023, China*
Lionel Guittat − *Laboratoire d'Optique et Biosciences (LOB), Ecole Polytechnique, CNRS, INSERM, Institut Polytechnique de Paris, Palaiseau 91120, France; Université Sorbonne Paris Nord, UFR SMBH, Bobigny 93000, France*
Wenli Zhang − *State Key Laboratory for Crop Genetics and Germplasm Enhancement and Utilization, CIC-MCP, Nanjing Agricultural University, Nanjing 210095, China;* orcid.org/0000-0003-0710-1966
David Monchaud − *Institut de Chimie Moléculaire de l'Université de Bourgogne (ICMUB), CNRS UMR6302, Université Bourgogne Europe (UBE), Dijon 21078, France;* orcid.org/0000-0002-3056-9295
Jean-Louis Mergny − *State Key Laboratory of Analytical Chemistry for Life Science, School of Chemistry and Chemical Engineering, Nanjing University, Nanjing 210023, China; Laboratoire d'Optique et Biosciences (LOB), Ecole Polytechnique, CNRS, INSERM, Institut Polytechnique de Paris, Palaiseau 91120, France;* orcid.org/0000-0003-3043-8401

Complete contact information is available at: https://pubs.acs.org/10.1021/jacs.5c01172

Author Contributions

#S.W., X.Z., and Y.F.contributed equally.

Notes

The authors declare no competing financial interest.

■ ACKNOWLEDGMENTS

We gratefully acknowledge the National Natural Science Foundation of China (22374070, 21977045, 22177047, 22004062, and 22104063), the State Key Laboratory of Analytical Chemistry for Life Science (5431ZZXM2406, SKLACLS2109, and SKLACLS2307), and the Fundamental Research Funds for the Central Universities (202200324, 202200325, and 020514380299).

■ REFERENCES

(1) Mergny, J. L.; Sen, D. DNA Quadruple Helices in Nanotechnology. *Chem. Rev.* **2019**, *119* (10), 6290−6325.
(2) McQuaid, K. T.; Pipier, A.; Cardin, C. J.; Monchaud, D. Interactions of small molecules with DNA junctions. *Nucleic Acids Res.* **2022**, *50* (22), 12636−12656.
(3) Hoyt, S. J.; Storer, J. M.; Hartley, G. A.; Grady, P. G. S.; Gershman, A.; de Lima, L. G.; Limouse, C.; Halabian, R.; Wojenski, L.; Rodriguez, M.; et al. From telomere to telomere: The transcriptional and epigenetic state of human repeat elements. *Science* **2022**, *376* (6588), No. eabk3112.
(4) Matos-Rodrigues, G.; Hisey, J. A.; Nussenzweig, A.; Mirkin, S. M. Detection of alternative DNA structures and its implications for human disease. *Mol. Cell* **2023**, *83* (20), 3622−3641.
(5) Weissensteiner, M. H.; Cremona, M. A.; Guiblet, W. M.; Stoler, N.; Harris, R. S.; Cechova, M.; Eckert, K. A.; Chiaromonte, F.; Huang, Y.-F.; Makova, K. D. Accurate sequencing of DNA motifs able to form alternative (non-B) structures. *Genome Res.* **2023**, *33* (6), 907−922.
(6) Bedrat, A.; Lacroix, L.; Mergny, J. L. Re-evaluation of G-quadruplex propensity with G4Hunter. *Nucleic Acids Res.* **2016**, *44* (4), 1746−1759.
(7) Hansel-Hertsch, R.; Di Antonio, M.; Balasubramanian, S. DNA G-quadruplexes in the human genome: Detection, functions and therapeutic potential. *Nat. Rev. Mol. Cell Biol.* **2017**, *18* (5), 279−284.
(8) Spiegel, J.; Cuesta, S. M.; Adhikari, S.; Hänsel-Hertsch, R.; Tannahill, D.; Balasubramanian, S. G-quadruplexes are transcription factor binding hubs in human chromatin. *Genome Biol.* **2021**, *22* (1), 117.
(9) Yu, Z.; Spiegel, J.; Melidis, L.; Hui, W. W. I.; Zhang, X.; Radzevičius, A.; Balasubramanian, S. Chem-map profiles drug binding to chromatin in cells. *Nat. Biotechnol.* **2023**, *41* (9), 1265−1271.
(10) Esnault, C.; Magat, T.; Zine El Aabidine, A.; Garcia-Oliver, E.; Cucchiarini, A.; Bouchouika, S.; Lleres, D.; Goerke, L.; Luo, Y.; Verga, D.; Lacroix, L.; Feil, R.; Spicuglia, S.; Mergny, J. L.; Andrau, J. C. G4access identifies G-quadruplexes and their associations with open chromatin and imprinting control regions. *Nat. Genet.* **2023**, *55* (8), 1359−1369.
(11) Song, J.; Gooding, A. R.; Hemphill, W. O.; Love, B. D.; Robertson, A.; Yao, L.; Zon, L. I.; North, T. E.; Kasinath, V.; Cech, T. R. Structural basis for inactivation of PRC2 by G-quadruplex RNA. *Science* **2023**, *381* (6664), 1331−1337.
(12) Sato, K.; Martin-Pintado, N.; Post, H.; Altelaar, M.; Knipscheer, P. Multistep mechanism of G-quadruplex resolution during DNA replication. *Sci. Adv.* **2021**, *7* (39), No. eabf8653.
(13) Dvorkin, S. A.; Karsisiotis, A. I.; Webba da Silva, M. Encoding canonical DNA quadruplex structure. *Sci. Adv.* **2018**, *4* (8), No. eaat3007.
(14) Phan, A. T. Human telomeric G-quadruplex: Structures of DNA and RNA sequences. *FEBS J.* **2010**, *277* (5), 1107−1117.
(15) Raguseo, F.; Wang, Y.; Li, J.; Petrić Howe, M.; Balendra, R.; Huyghebaert, A.; Vadukul, D. M.; Tanase, D. A.; Maher, T. E.; Malouf, L.; et al. The ALS/FTD-related C9orf72 hexanucleotide repeat expansion forms RNA condensates through multimolecular G-quadruplexes. *Nat. Commun.* **2023**, *14* (1), 8272.
(16) Trachman, R. J., III; Demeshkina, N. A.; Lau, M. W. L.; Panchapakesan, S. S. S.; Jeng, S. C. Y.; Unrau, P. J.; Ferre-D'Amare, A. R. Structural basis for high-affinity fluorophore binding and activation by RNA Mango. *Nat. Chem. Biol.* **2017**, *13* (7), 807−813.
(17) Varshney, D.; Spiegel, J.; Zyner, K.; Tannahill, D.; Balasubramanian, S. The regulation and functions of DNA and RNA G-quadruplexes. *Nat. Rev. Mol. Cell Biol.* **2020**, *21* (8), 459−474.
(18) Lyu, K.; Chow, E. Y.-C.; Mou, X.; Chan, T.-F.; Kwok, C. K. RNA G-quadruplexes (rG4s): Genomics and biological functions. *Nucleic Acids Res.* **2021**, *49* (10), 5426−5450.
(19) Dumas, L.; Herviou, P.; Dassi, E.; Cammas, A.; Millevoi, S. G-quadruplexes in RNA biology: Recent advances and future directions. *Trends Biochem. Sci.* **2021**, *46* (4), 270−283.
(20) Tassinari, M.; Richter, S. N.; Gandellini, P. Biological relevance and therapeutic potential of G-quadruplex structures in the human noncoding transcriptome. *Nucleic Acids Res.* **2021**, *49* (7), 3617−3633.
(21) Li, F.; Zhou, J. G-quadruplexes from non-coding RNAs. *J. Mol. Med.* **2023**, *101* (6), 621−635.
(22) Robinson, J.; Raguseo, F.; Nuccio, S. P.; Liano, D.; Di Antonio, M. DNA G-quadruplex structures: More than simple roadblocks to transcription? *Nucleic Acids Res.* **2021**, *49* (15), 8419−8431.
(23) Kwok, C. K.; Marsico, G.; Sahakyan, A. B.; Chambers, V. S.; Balasubramanian, S. rG4-seq reveals widespread formation of G-quadruplex structures in the human transcriptome. *Nat. Methods* **2016**, *13* (10), 841−844.

(24) Lam, S. Y.; Umar, M. I.; Zhao, H.; Zhao, J.; Kwok, C. K. Capture of RNA G-quadruplex structures using an $_L$-RNA aptamer. *RSC Chem. Biol.* **2024**, *5* (10), 1045−1051.
(25) Yang, S. Y.; Lejault, P.; Chevrier, S.; Boidot, R.; Robertson, A. G.; Wong, J. M. Y.; Monchaud, D. Transcriptome-wide identification of transient RNA G-quadruplexes in human cells. *Nat. Commun.* **2018**, *9* (1), 4730.
(26) Weng, X.; Gong, J.; Chen, Y.; Wu, T.; Wang, F.; Yang, S.; Yuan, Y.; Luo, G.; Chen, K.; Hu, L.; Ma, H.; Wang, P.; Zhang, Q. C.; Zhou, X.; He, C. Keth-seq for transcriptome-wide RNA structure mapping. *Nat. Chem. Biol.* **2020**, *16* (5), 489−492.
(27) Mitteaux, J.; Raevens, S.; Wang, Z.; Pirrotta, M.; Valverde, I. E.; Hudson, R. H. E.; Monchaud, D. PhpC modulates G-quadruplex-RNA landscapes in human cells. *Chem. Commun.* **2024**, *60* (4), 424−427.
(28) Yang, S. Y.; Monchaud, D.; Wong, J. M. Y. Global mapping of RNA G-quadruplexes (G4-RNAs) using G4RP-seq. *Nat. Protoc.* **2022**, *17* (3), 870−889.
(29) Mitteaux, J.; Monchaud, D. Protocol for cellular RNA G-quadruplex profiling using G4RP.v2. *STAR Protoc.* **2024**, *5* (4), 103480.
(30) Varshney, D.; Cuesta, S. M.; Herdy, B.; Abdullah, U. B.; Tannahill, D.; Balasubramanian, S. RNA G-quadruplex structures control ribosomal protein production. *Sci. Rep.* **2021**, *11* (1), 22735.
(31) Surani, A. A.; Montiel-Duarte, C. Native RNA G quadruplex immunoprecipitation (rG4IP) from mammalian cells. *STAR Protoc.* **2022**, *3* (2), 101372.
(32) Dai, Q.; Ye, C.; Irkliyenko, I.; Wang, Y.; Sun, H.-L.; Gao, Y.; Liu, Y.; Beadell, A.; Perea, J.; Goel, A.; He, C. Ultrafast bisulfite sequencing detection of 5-methylcytosine in DNA and RNA. *Nat. Biotechnol.* **2024**, *42* (10), 1559−1570.
(33) Gallego Romero, I.; Pai, A. A.; Tung, J.; Gilad, Y. RNA-seq: Impact of RNA degradation on transcript quantification. *BMC Biol.* **2014**, *12* (1), 42.
(34) Manioglu, S.; Modaresi, S. M.; Ritzmann, N.; Thoma, J.; Overall, S. A.; Harms, A.; Upert, G.; Luther, A.; Barnes, A. B.; Obrecht, D.; et al. Antibiotic polymyxin arranges lipopolysaccharide into crystalline structures to solidify the bacterial membrane. *Nat. Commun.* **2022**, *13* (1), 6195.
(35) Paterson, D. L.; Harris, P. N. Colistin Resistance: A Major Breach in Our Last Line of Defence. *Lancet Infect Dis.* **2016**, *16* (2), 132−133.
(36) Bugaut, A.; Balasubramanian, S. 5′-UTR RNA G-quadruplexes: Translation regulation and targeting. *Nucleic Acids Res.* **2012**, *40* (11), 4727−4741.
(37) Jia, L.; Mao, Y.; Ji, Q.; Dersh, D.; Yewdell, J. W.; Qian, S.-B. Decoding mRNA translatability and stability from the 5′UTR. *Nat. Struct. Mol. Biol.* **2020**, *27* (9), 814−821.
(38) Roschdi, S.; Yan, J.; Nomura, Y.; Escobar, C. A.; Petersen, R. J.; Bingman, C. A.; Tonelli, M.; Vivek, R.; Montemayor, E. J.; Wickens, M.; Kennedy, S. G.; Butcher, S. E. An atypical RNA quadruplex marks RNAs as vectors for gene silencing. *Nat. Struct. Mol. Biol.* **2022**, *29* (11), 1113−1121.
(39) Yang, Q.-F.; Wang, X.-R.; Wang, Y.-H.; Wu, X.-H.; Shi, R.-Y.; Wang, Y.-X.; Zhu, H.-N.; Yang, S.; Tang, Y.-L.; Li, F. G4LDB 3.0: Database for discovering and studying G-quadruplex and i-motif ligands. *Nucleic Acids Res.* **2025**, *53* (D1), D91−D98.
(40) Ranjan, N.; Andreasen, K. F.; Kumar, S.; Hyde-Volpe, D.; Arya, D. P. Aminoglycoside binding to Oxytricha nova telomeric DNA. *Biochemistry* **2010**, *49* (45), 9891−9903.
(41) Martino, L.; Virno, A.; Pagano, B.; Virgilio, A.; Di Micco, S.; Galeone, A.; Giancola, C.; Bifulco, G.; Mayol, L.; Randazzo, A. Structural and thermodynamic studies of the interaction of distamycin A with the parallel quadruplex structure $[d(TGGGGT)]_4$. *J. Am. Chem. Soc.* **2007**, *129* (51), 16048−16056.
(42) Chung, W. J.; Heddi, B.; Schmitt, E.; Lim, K. W.; Mechulam, Y.; Phan, A. T. Structure of a left-handed DNA G-quadruplex. *Proc. Natl. Acad. Sci. U. S. A.* **2015**, *112* (9), 2729−2733.
(43) Bian, Y.; Lv, F.; Pan, H.; Ren, W.; Zhang, W.; Wang, Y.; Cao, Y.; Li, W.; Wang, W. Fusion dynamics and size-dependence of droplet microstructure in ssDNA-mediated protein phase separation. *JACS Au.* **2024**, *4* (9), 3690−3704.
(44) Mimura, M.; Tomita, S.; Shinkai, Y.; Hosokai, T.; Kumeta, H.; Saio, T.; Shiraki, K.; Kurita, R. Quadruplex folding promotes the condensation of linker histones and DNAs via liquid-liquid phase separation. *J. Am. Chem. Soc.* **2021**, *143* (26), 9849−9857.
(45) Alzeer, J.; Vummidi, B. R.; Roth, P. J.; Luedtke, N. W. Guanidinium-modified phthalocyanines as high-affinity G-quadruplex fluorescent probes and transcriptional regulators. *Angew. Chem., Int. Ed.* **2009**, *48* (49), 9362−9365.
(46) Kuryavyi, V.; Phan, A. T.; Patel, D. J. Solution structures of all parallel-stranded monomeric and dimeric G-quadruplex scaffolds of the human c-kit2 promoter. *Nucleic Acids Res.* **2010**, *38* (19), 6757−6773.
(47) Gregoire, N.; Aranzana-Climent, V.; Magreault, S.; Marchand, S.; Couet, W. Clinical pharmacokinetics and pharmacodynamics of colistin. *Clin. Pharmacokinet.* **2017**, *56* (12), 1441−1460.
(48) Mitra, J.; Makurath, M. A.; Ngo, T. T. M.; Troitskaia, A.; Chemla, Y. R.; Ha, T. Extreme mechanical diversity of human telomeric DNA revealed by fluorescence-force spectroscopy. *Proc. Natl. Acad. Sci. U. S. A.* **2019**, *116* (17), 8350−8359.
(49) Johnson, S. A.; Paul, T.; Sanford, S. L.; Schnable, B. L.; Detwiler, A. C.; Thosar, S. A.; Van Houten, B.; Myong, S.; Opresko, P. L. BG4 antibody can recognize telomeric G-quadruplexes harboring destabilizing base modifications and lesions. *Nucleic Acids Res.* **2024**, *52* (4), 1763−1778.

https://doi.org/10.1021/jacs.5c01172
J. Am. Chem. Soc. 2025, 147, 9962−9971